Relaxation of photon echoes in weakly ionized noble-gas plasmas

T. Baer
Department of Physics, University of Chicago, Chicago, Illinois 60637
(Received 19 March 1979)

Photon echoes generated from visible transitions in the noble gases helium, neon, and argon are observed and the collisional relaxation rates are measured. The photon echoes are excited on transitions initiating from metastable states which are populated by electron impact in an rf discharge. The photon-echo intensity is measured as a function of time after the discharge is turned off and as a function of gas pressure. The reduction of the echo intensity in these two experiments is attributed to relaxation of the metastable population in the afterglow and dephasing collisions, respectively. The dependence of the photon-echo damping time on transition wavelength and perturber gas is interpreted by means of a simple van der Waals model for the excited-atom and perturber-gas interaction.

INTRODUCTION

Photon echoes have been observed in a number of solids and gases since their initial observation in ruby by Abella *et al.*[1-9] These previous studies have primarily used the photon echo to measure the persistence of optical coherence in the media after pulsed resonant excitation. The photon echo has, however, also provided atomic structure information such as hyperfine splittings and g factors.[10-13] The present work applies the photon-echo method to study the collision dynamics of a weakly ionized plasma and thus introduces a new class of materials which can be probed using this technique.

In this paper the results of photon-echo experiments done on the noble gases helium, neon, and argon, in a weak rf discharge are presented. Relaxation of the echo signal as a function of time after the discharge is shut off is shown to arise from depopulation of the metastable states, and relaxation as a function of gas pressure is attributed to dephasing collisions in the plasma. This paper, and a previous preliminary letter,[14] are the first reports of observations of photon echoes in the noble gases.

The photon-echo relaxation times are compared with previous line broadening[15,16] and absorption experiments[17-19] which measure related decay processes in plasmas. The photon-echo probe can supplement these traditional spectroscopic diagnostic techniques which are more applicable at higher pressures where pressure broadening and resonant absorption processes are large. The echo technique, in contrast, is most useful at pressures less than one Torr, where pressure broadening is small compared to the Doppler width, and the medium is optically thin.

The collisional damping of photon echoes generated on vibrational transitions in molecular gases has been studied in a number of experiments. Patel and Slusher[3] made the first measurements in SF_6 using a pulsed CO_2 laser. Subsequent experiments were done by Brewer and Shoemaker[4] in $^{13}CH_3F$ and NH_2D, Alimpiev and Karlov[5] in BCL_3 and SF_6, Heer and Nordstrom[6] in SF_6, and Berman *et al.*[7] in $^{13}CH_3F$. Berman *et al.*[7] have demonstrated that the damping of photon echoes generated on vibrational transitions is primarily caused by velocity changing collisions.

Echoes generated on electronic transitions, in contrast, are primarily damped by dephasing collisions.[7] These damping rates have been measured in iodine[8] and sodium,[9] but no theoretical predictions of the observed rates have been presented.

Therefore, part of the motivation for these experiments was to measure photon-echo relaxation excited on electronic states in a number of different elements in order to search for systematics in the decay times. Using the weak plasma environment, we investigate a variety of transitions from metastable states in the noble gases; their wavelengths range from the near ultraviolet to the deep red. The predominant species in the noble-gas plasma is the ground-state noble-gas atom, i.e., photon echoes observed in helium are damped by collisions with helium ground-state atoms, those in neon by neon ground-state atoms, etc. Thus the dependence of the observed rates on perturber gas can also be inferred.

The photon-echo relaxation times are compared with dipole-moment damping times calculated using a simple line-broadening theory. The calculated dipole damping times for transitions in the noble gases predict the general trends of the photon-echo decay times as a function of transition wavelength and perturber polarizability. The same theory is used to predict photon-echo damping times in sodium-argon mixtures, which were recently measured by Flusberg *et al.*[9]

In the experiments reported here the echoes are

venient method of photon-echo polarization rotation by a magnetic field.[12] This technique eliminates the need for precise synchronization of optical shutters with the pulsed laser and considerably simplifies the experiment.

Section I reviews the properties of the echo signal relevant to the present experiment. Section II describes the experimental apparatus. Section III contains the results of metastable lifetime measurements and comparison with other experiments. Section IV presents optical coherence relaxation experiments, and Sec. V compares the photon echo data with line-broadening experiments and theory.

I. REVIEW OF PHOTON-ECHO PROPERTIES

The properties of the echo signal which are important in the present experiments are summarized below. For additional details the reader is referred to a number of monographs which present theoretical treatments of the details of photon echo emission.[1,12,20]

A photon-echo signal is generated in a sample by applying two collinear pulses resonant with a dipole transition and separated by a time interval τ. The sample emits the photon echo signal at a time $t=2\tau$ after the first pulse. This signal is characterized by a highly collimated emission of light propagating collinear to the excitation pulses with a pulse width which is usually equal to that of the exciting pulses.

The first excitation pulse creates a nonstationary superposition state in the atoms of the gas sample. The expectation value of the dipole-moment operator is finite for this state and it oscillates in time at the resonance frequency. The dipole moments at different locations in the sample initially oscillate coherently and are summed to determine the overall light intensity emitted by the sample immediately after the first pulse. The light emitted by the sample immediately after the first laser excitation is a coherent pulse similar to the echo signal as described above and is usually referred to as the free-induction signal.[20] The atomic dipole moments quickly lose their initial phase coherence because of Doppler broadening, thus damping this induction signal. This process is normally called free-induction decay.

The second excitation pulse, at $t=\tau$, changes the phase of the atomic superposition states and returns, at $t=2\tau$, the dephased dipole moments to their initial, $t=0$, coherent phase relationship. The echo signal is thus the light emitted by the rephased coherent atomic dipole moments and is an "echo" of the free-induction signal emitted after the first pulse.

Typically, one observes the echo signal *intensity* which is proportional to the square of the coherent sum of the expectation value of the atomic dipole moments evaluated at $t=2\tau$,

$$I_{\text{echo}} \propto \left| \sum_i \langle \vec{p}_i(2\tau) \rangle \right|^2 , \tag{1}$$

where $\vec{p}_i$ stands for the dipole operator, and we are summing over all atoms at their various locations in the sample. Since the dipole-moment amplitudes are summed coherently, the echo intensity is proportional to the *square* of the number density of emitting atoms.

Collinear excitation is necessary in a gas because of an additional dephasing of the photon echo due to the Doppler motion of the atoms.[21] This dephasing factor damps the echo-signal intensity rapidly and depends critically on the angle between the excitation pulse propagation vectors.[13] To observe the echo signal in a gas one is, in practice, restricted to collinear excitation.

If both excitation pulses are plane polarized in the same direction, the echo is normally emitted polarized paralled to this direction. However, a magnetic field parallel to the propagation vector of the incident pulses will generally rotate the polarization direction of the echo-signal.[12]

In general, the photon echo polarization is parallel to the direction of the electric dipole moment evaluated at $t=2\tau$. The expectation value of the dipole moment at $t=2\tau$ is most easily determined from the density matrix for an atom subjected to two resonant pulses while in a magnetic field. Details of this magnetic rotation effect have been discussed in a previous paper.[12]

The rotation of the echo polarization arises from the precession of the atomic magnetic moments about the applied field direction. As a result of this precession, the electric dipole rotates from its zero magnetic field direction and the photon-echo signal is emitted polarized at an angle with respect to the excitation pulse polarization. We use this effect to simplify detection of the photon echoes as described in Sec. II.

Photon-echo emission depends on the existence of a coherent atomic dipole moment in the gas sample at $t=2\tau$. Random thermal collisions damp the coherent dipole moment created by the laser pulses, thus decreasing the photon-echo signal. This damping is generally represented as a simple exponential function of time.[20] This approximation is equivalent to assuming that all off-diagonal elements of the atomic density matrix, which connect the upper and lower states of the transition, decay at the same rate.[22] We employ this approximation in the treatment of the experimental data reported here and discuss its validity in Sec. V. The relaxa-

tion time of the echo signal will be referred to as T_2 and will be called the optical-coherence damping time.

II. EXPERIMENTAL DESIGN

Figure 1 contains a schematic of the experimental apparatus. The two laser excitation pulses are obtained from a N_2 laser pumped dye laser. Part of the dye laser output is delayed for 15–60 nsec in one of two White-cell delay lines.[1] The original and delayed dye laser pulses are made collinear at a second beam splitter. The laser light is linearly polarized by a Glan-Thompson prism immediately before the sample cell. After the cell a second polarizer is aligned with its pass axis orthogonal to the first polarizer, thus blocking the laser pulses from the detector. The echo is observed using the polarization-rotation effect described in Sec. I.

The nitrogen laser is a "fast pulse" National Research Group model .5-5-150. Its pulse width is 5 nsec and peak power is 500 kW. The laser was modified to be triggerable by replacing the free running spark gap with a hydrogen thyraton (EGG HY1102).

The dye laser is a grazing incidence grating design after Littman *et al.*[23] Two gratings, one at grazing incidence and the other in Littrow mount, are employed, and the linewidth and power are estimated to be similar to those measured by Littman *et al*[23]: a few GHz and about 1 kW, respectively. The dye-laser pulse width is about 2 nsec. This dye-laser design replaces a Hänsch-type dye laser[24] with intracavity telescope and etalon which was used in earlier photon-echo studies.[12] The grazing incidence laser has performed quite well and is much easier to align.

As shown in Fig. 1, the experimental design incorporates two delay lines which can be adjusted separately. A particular delay line is selected by opening or closing either of two diaphragms in the beam line. The photon-echo intensity can thus be measured at different delays without adjustment of any optical components. This experimental design facilitates measurement of the optical coherence decay rate as discussed further in Sec. IV.

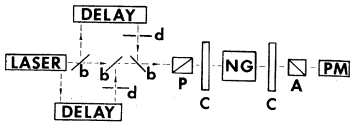

FIG. 1. Schematic diagram of the experimental apparatus where b indicates beam splitters, d is a diaphragm, P and A are polarizer and analyzer, C is a Helmholtz coil, NG stands for noble gas, and PM is a photomultiplier.

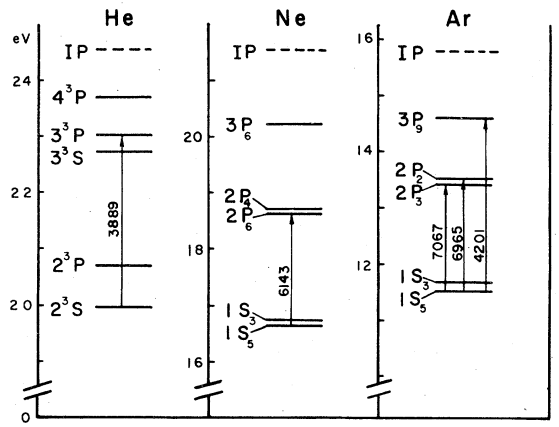

FIG. 2. Energy-level diagram of some of the relevant levels in helium, neon, and argon. The transitions which were used to generate echo signals are indicated by arrows with the wavelength listed in A. Paschen notation is used to specify the various levels in neon and argon as in Ref. 25. The levels 2^3S in helium and $1S_5$ in neon and argon are metastable.

The discharge cell is cylindrical with a 2-cm diameter and 5-cm length. The cell is connected to a vacuum system through which a noble gas can be flowed. A MKS capacitance manometer (type 222) determines the gas pressure to ±2%. A few-watt 50-MHz rf oscillator powers the noble-gas discharge. The rf power is coupled into the cell by copper tape electrodes on the outside of the cell. The cell temperature does not change when the discharge is on, and thus we assume that all experiments were performed at room temperature (300°K).

The rf discharge can be turned off in less than a microsecond by applying a fast rise-time rectangular pulse to the screen of the oscillator tube. This technique is used to study relaxation of the photon echo as a function of time after the discharge has been stopped, as described in Sec. III.

The cell is located between two Helmholtz coils which produce a magnetic field parallel to the propagation direction of the laser pulses. The crossed polarizers block the laser pulses from the photomultiplier, but the echo polarization rotates due to the magnetic field, and thus the echo signal is detected. The value of the magnetic field which provides the maximum rotated echo signal depends on the Landé g factors of the states involved,[12] but is typically between 5 and 10 G. At higher fields, Faraday rotation of the excitation pulses reduces the signal to noise ratio.[13]

The photomultiplier (RCA 1P28A or 7265) signal is fed into a linear gate (Chronetics 116) which passes only the echo signal, eliminating noise

due to scattered laser light. The linear gate also stretches the echo signal, and this stretched output is pulse-height analyzed. Typical data points are the averages of 600–1000 laser shots.

The uncertainty of the photon-echo relaxation times, using the polarization rotation technique, is estimated to be roughly ±20%. Most of this uncertainty comes from pulse-to-pulse jitter of the dye laser output and from a limitation on the measurable range of the photon-echo intensities because of background light from the laser and discharge. The scattered light background could be significantly reduced by incorporating Kerr's or Pockel's cell shutters as in previous experiments,[1] although this would considerably complicate the experiment.

Figure 2 contains term diagrams for helium, neon, and argon[25] showing the transitions involved in the photon-echo emission. The states in neon and argon are labeled using the Paschen notation.[25] The metastable states 2^3S and $1S_5$ are about 12–20 eV above the ground state. These states are forbidden to radiate to the ground state in a dipole process by angular momentum selection rules. All the experiments used transitions from the metastable states in the visible spectrum. Typical radiative lifetimes of the excited states in neon and argon were 20 ~ 30 nsec.[26] In helium the 3^3P state has a lifetime of 100 nsec.[26]

The metastable states are populated by electron impact in the discharge. The lifetimes of the metastable states are limited by collisions with ground-state atoms, with free ions or electrons, and with the walls.[17–19] Weak rf plasmas typically have such a low fractional ionization (~10^{-6}), that collisions of metastables with charged species are negligible, and the most probable collision is with a ground-state noble-gas atom.[19] This assumption is consistent with the experimental results presented below. The number density of metastable atoms[19] is typically around 10^9–10^{10} cm^{-3}.

III. RELAXATION OF THE PHOTON ECHO IN THE DISCHARGE AFTERGLOW

If the rf discharge is shut off quickly the number density of metastable atoms decays in time due to collisions with ground-state noble-gas atoms or the walls. The time and spatial dependence of the metastable number density $N^*(\vec{r}, t)$ is given by a simple diffusion equation

$$\frac{\partial}{\partial t}[N^*(\vec{r}, t)] = D\nabla^2 N^*(\vec{r}, t) - \nu_c N^*(\vec{r}, t), \tag{2}$$

where D is a diffusion constant, ν_c a collision rate, and $\vec{r}$ specifies a particular volume element in the cell.[17–19] The first term on the right-hand side of Eq. (2) represents the process of diffusion of the metastable atoms through the ground-state noble-gas atoms and subsequent relaxation at the walls of the container. D is the diffusion constant for this process and is *inversely proportional* to the pressure in the discharge cell. The collision term ν_c represents losses due to two- and three-body collisions and is thus *directly proportional* to integer powers of the pressure.

Equation (2) is valid when the mean free path of the atoms in the gas is much smaller than the characteristic dimensions of the container. This approximation is quite justified at the pressures (10^{-1} Torr) and container dimensions (a few cm) used in this experiment.

The solution to Eq. (2) is a sum of the form[27]

$$N^*(\vec{r}, t) = \sum_{k=1}^{\infty} \exp(-\Gamma_k t) f_k(\vec{r}). \tag{3}$$

Each term is a distinct diffusion mode with $f_k(\vec{r})$ the spatial distribution of the metastable number density for this mode. The functions $f_k(\vec{r})$ are determined by enforcing the boundary conditions, which are that the metastable number density be zero at the container walls.

For cylindrical containers the functions $f_k(\vec{r})$ are products of trigonometric and Bessel functions. The higher diffusion modes ($k > 1$) have very fast relaxation times, and the dominant decay mode after a short period of time is the lowest mode ($k = 1$).[27] For this mode one finds that

$$\Gamma_1 = (D/\Lambda^2) + \nu_c, \tag{4}$$

where Λ^2 is the diffusion length for the sample cell and is given by

$$\Lambda^{-2} = (\pi^2/L^2) + (5.81/a^2), \tag{5}$$

where L is the length and a is the radius of the cell.

The loss of metastable population will affect the photon-echo intensity since the echo is proportional to the square of the metastable number density. The time of the photon-echo experiment is about 30 nsec, which is much shorter than the typical 50-μsec decay time of N^*. Thus to a good approximation N^* does not change over the time of the echo experiment. If we vary the time at which we probe with the echo excitation pulses after the discharge is off, the echo intensity emitted from a point $\vec{r}$ in the sample will be given by

$$I_{\text{echo}} \propto [N^*(\vec{r}, t)]^2 \propto [N_0^*(\vec{r})]^2 \exp(-2\Gamma_1 t), \tag{6}$$

where t is the time after the discharge has been turned off and $N_0^*(\vec{r})$ is the initial metastable number density. Thus the photon-echo signal will de-

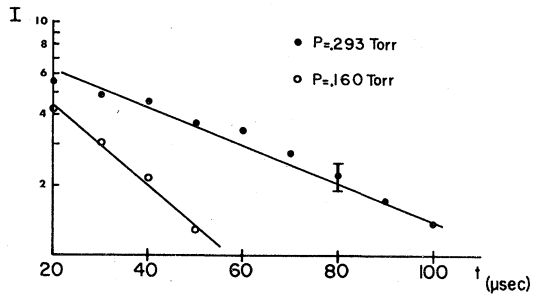

FIG. 3. Graph of the intensity (in arbitrary units) of the photon-echo signal emitted by helium at 3889 Å vs the time after the discharge has been shut off. The lines are least-squares fits to the experimental data.

cay at twice the metastable damping rate.

Figure 3 shows results of experiments in helium done at two different pressures. The abscissa is the time t at which the echo was excited after cessation of the discharge. The ordinate is the intensity of the echo in arbitrary units. The data in Fig. 3 indicate that the metastable atoms appear to decay as a single exponential in time and that the decay rate *decreases* with increasing pressure. Thus the dominant term in Eq. (4) is the diffusion term. Results of resonant absorption experiments done at higher pressures indicate that the two- and three-body collision loss rates at ~0.20 Torr are indeed negligible.[17-19]

Table I summarizes results of experiments done in helium, neon, and argon. The decay rates were calculated by least-squares fitting single-exponential decay functions to the experimental data. The diffusion constants were calculated using Eq. (4) and neglecting the collision term. Table I also contains the results of previous experiments, generally performed at higher pressures, where the metastable decay rate was measured by resonance absorption from the metastable state.[17-19]

The total error in the diffusion constants is estimated to be ±20%. This includes estimates of the statistical error due to pulse-to-pulse jitter in the dye laser and possible systematic errors caused by background gas impurities in the sample cell. The diffusion constants measured in these experiments are consistent with the previous measurements.[17-19]

Thus the photon-echo signal can be used to measure metastable state lifetimes and diffusion constants in a plasma. The photon-echo experiments have the advantage of high signal-to-noise ratio at low number densities and low optical thickness.

IV. RELAXATION OF THE PHOTON ECHO DUE TO DEPHASING COLLISIONS

If we assume that the overall effect of dephasing collisions is an exponential damping in time of the echo signal, then the echo intensity will depend on the metastable number density and the time between laser pulses according to

$$I_e \propto (N^*)^2 \exp(-4\tau/T_2), \tag{7}$$

where N^* is the metastable number density integrated over the excitation region, and τ is the delay between the laser pulses.[20] N^* is assumed to be constant over the time of the echo experiment.

T_2 usually refers to the relaxation rate of the off-diagonal elements of the density matrix.[20] Since the echo is proportional to the square of these terms evaluated at $t = 2\tau$, we include a factor of four in Eq. (7).

If binary collisions between the excited metastable and ground-state noble-gas atoms are the predominant decay mechanism, then T_2 will be inversely proportional to the noble-gas pressure. In past experiments T_2 has been measured by holding N^* constant and measuring I_e as a function of a background gas pressure P.[9] In the discharge this is not possible since the metastable density N^* is itself a sensitive function of the noble-gas

TABLE I. Metastable lifetimes and calculated diffusion constants.

State	Measured lifetime $1/\Gamma_1$ (μsec)	Diffusion constant at 1 Torr D(cm²/s)	Other Expt. D(cm²/s)
He 2^3S	50 ± 10 (0.160 Torr)	390 ± 80	470[a] ± 25
Ne $1S_5$	83 ± 20 (0.156 Torr)	204 ± 40	170[b] ± 10
Ar $1S_5$	248 ± 50 (0.80 Torr)	45 ± 9	52[c] 48 40

[a] A. V. Phelps (Ref. 18).
[b] Dixon and Grant (Ref. 17).
[c] From Table 5.11 of J. L. Delcroix *et al.* (Ref. 19).

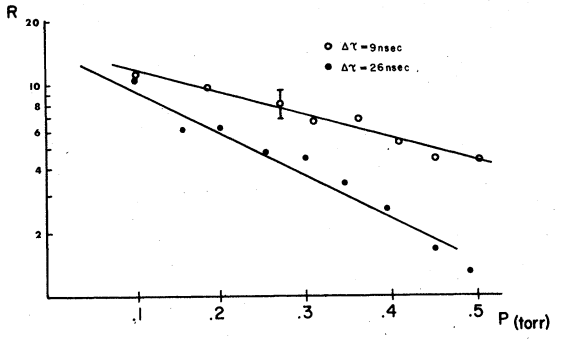

FIG. 4. Graph of the ratio of echo intensity in arbitrary units vs pressure for the 7607-Å line of argon.

pressure P. We indicate this by writing the metastable number density as $N^*(P)$.

This problem is overcome by performing the echo experiment at two different time delays τ_1 and τ_2 at the same pressure. The ratio of the observed signals is

$$R \propto \frac{N^*(P)\exp(-4\tau_1/T_2)}{N^*(P)\exp(-4\tau_2/T_2)} \propto \exp\left(\frac{-4\Delta\tau}{T_2}\right), \qquad (8)$$

where $\Delta\tau = \tau_1 - \tau_2$. The ratio R is thus independent of $N^*(P)$. This ratio is measured at a series of different pressures, and fitting an exponential curve to the plot of R versus pressure determines T_2.

The experimental design for measuring T_2 was discussed briefly in Sec. II. Two adjustable delay lines produce pulses at the desired values of τ_1 and τ_2, and either delay is selected by opening or closing two diaphragms. Data are taken at both delays sequentially at a certain pressure; the pressure is then changed and the experiment repeated. The finite lifetime of the excited states due to spontaneous decay and collision relaxation restricts the delays to be $\lesssim 60$ nsec.

Figure 4 shows some typical data from the 7067-A ($1S_5 \rightarrow 2P_3$) line in argon. R appears to decay exponentially with the pressure. The experimental data in Fig. 4 are the results of two experiments with different $\Delta\tau$, and R decays faster as $\Delta\tau$ is increased as predicted by Eq. (8).

Table II contains a summary of experiments in helium, neon, and argon on a number of transitions. T_2 is expressed in units of nsec Torr and, if it is divided by the pressure, gives the damping time at that pressure. In general, T_2 is independent of $\Delta\tau$ to within the estimated experimental error. The value of T_2 measured in helium is consistent with previous measurements which assumed $N^*(P)$ to depend linearly on P.[14]

It is interesting to note that the photon-echo signal supplies information about two very different effective cross sections of the metastable atom. The diffusion constant D can be used to calculate a kinetic cross section

$$\sigma_1 = (3\pi/32)(\bar{V}/nD), \qquad (9)$$

where n is the number density of ground-state atoms in the plasma.[17] This cross section is essentially the effective size of the metastable atom with respect to collisions which transfer a significant amount of momentum. On the other hand, T_2 can be used to calculate the effective size of the atom with respect to changing the phase of the atomic dipole moment. This cross section is

$$\sigma_2 = (n\bar{V}T_2)^{-1}. \qquad (10)$$

For example, in neon $\sigma_1 = 3.6\times 10^{-15}$ cm^2 and $\sigma_2 = 1.9\times 10^{-14}$ cm^2. In general, σ_2 is larger than σ_1, for the noble-gas transitions studied here σ_2/σ_1 ranges from ~3 to 20.

The data in Table II indicate that the shorter wavelength transitions have faster damping rates, and that ground-state argon atoms are a particularly effective damping agent. These conclusions are consistent with measurements of the relaxation of the atomic dipole moment in line-broadening experiments performed in the noble gases.[15]

A comparison of line-broadening and photon-echo experiments will be presented in Sec. V.

TABLE II. Measurements of T_2 from photon-echo and line-broadening experiments and results of the theoretical calculation.

		Photon echo	Line broadening	
		T_2	Experiment	Theory
	λ(Å)	(nsec-Torr)	(nsec-Torr)	(nsec-Torr)
Helium	3889	6.0 ± 1.5	···	10.7
Neon	6143	21.0 ± 5	···	28
	5945	···	19.0 ± 2[a]	28
Argon	7067	22.0 ± 5	···	16
	6965	19.0 ± 5	19.7 ± 0.6[b]	16
			16.0 ± 2.5[c]	
	4200	2.5 ± 0.5	···	7.6

[a] Kuhn (Ref. 15).
[b] Stacey and Vaughan (Ref. 16).
[c] Hindmarsh and Thomas (Ref. 16).

V. COMPARISON OF LINE-BROADENING AND PHOTON-ECHO EXPERIMENTS

A. Relation of line-broadening constants to T_2

Pressure broadening of electronic transitions, where velocity changing and quenching collisions can often be neglected, is caused by dephasing

TABLE III. Photon-echo relaxation in Na.

Transition	T_2 (nsec-Torr) Theory	Expt.[a]
$3S_{1/2} \rightarrow 3P_{1/2}$	23	17.0 ± 1.3
$3P_{1/2} \rightarrow 5S_{1/2}$	7.3	4.8 ± 0.3
$3P_{1/2} \rightarrow 6S_{1/2}$	4.8	2.8 ± 0.3
$3P_{1/2} \rightarrow 4D_{3/2}$	7.0	6.0 ± 0.3
$3P_{1/2} \rightarrow 5D_{3/2}$	4.5	3.5 ± 0.3
$3P_{1/2} \rightarrow 6D_{3/2}$	3.4	2.4 ± 0.2
$3P_{1/2} \rightarrow 7D_{3/2}$	2.7	1.8 ± 0.9

[a] Flusberg *et al.* (Ref. 9).

observed using the particularly simple and concollisions which damp the atomic dipole moment amplitude.[28-30] Most theoretical treatments of line broadening employ the binary collision and impact approximations which assume that the time length of a binary collision is much shorter than the time between collisions or any other atomic time scales in the problem (except the optical frequency).[29] This approximation is quite accurate within a few wave numbers of line center at pressures at or beneath 10 Torr. Given this assumption the dipole moment can be shown to decay exponentially because of collisions.[28,30]

By fitting a single-exponential function to the echo data we have implicitly assumed that all off-diagonal elements of the density matrix decay at the same rate. Thus within the limits of accuracy of this assumption, the dipole-moment decay rate should equal $1/T_2$ since the dipole moment is also proportional to these off-diagonal elements of the density matrix.

The exponential decay of the dipole moment gives rise to the familiar Lorentz line shape which is the intensity profile of the light—not including Doppler or radiative broadening.[30] The relation between the full width at half-maximum (FWHM) of a pressure-broadened line, and the decay rate of the dipole moment is given by

$$\Gamma_{DM} = \pi \Delta \nu_{FWHM}. \tag{11}$$

In practice $\Delta \nu_{FWHM}$ is determined by fitting a Voigt profile to the observed line shape which normally is Doppler, radiative, and pressure broadened. The radiative contribution is determined by extrapolating the measured line shapes to zero pressure. The pressure-broadening contribution is determined from the variation of the observed line shape with pressure.[15]

Equation (11) can be used to compare the experimental line-broadening constant ($\Delta \nu_{FWHM}$) with values of T_2 measured in photon-echo experiments.

Line-broadening experiments have been performed previously on a few transitions in the noble gases,[15,16] and the results for some lines in argon and neon are listed in Table II. Though no quantitative measurement of the 6143-Å ($1S_5 - 2P_6$) line-broadening constant in neon appears to have been made, experiments indicate that transitions from this fine-structure multiplet to the $1S_5$ metastable level are broadened equally.[31] Thus we expect that the 5945-Å ($1S_5 - 2P_4$) line-broadening constant will be equal to or slightly greater than its value for the 6143-Å line.

The results in Table III indicate that the values of T_2 measured in the photon echo experiments are equal to the dipole-moment decay rate measured in line-broadening experiments to within the error of both types of experiments.

B. Use of line-broadening theory to estimate T_2

The comparison of line-broadening and photon-echo experiments in Table II suggests that line-broadening theories can be used successfully to predict photon-echo relaxation rates in gases. We present below a particularly simple line-broadening calculation which represents the excited atom and perturber interaction as a van der Waals potential. We first outline the theoretical model and then compare the theoretical predictions with photon-echo relaxation data. This theoretical treatment is discussed in greater detail by Hindmarsh and Farr in their recent review article.[29]

In this model the interaction between the radiating atom and the perturber is assumed to be an R^{-6} or van der Waals interaction

$$V_i(R) = C_6^i / R^6, \tag{12}$$

where i refers to either the upper (u) or lower (l) state and R is the internuclear separation. The upper and lower states have different interatomic potential curves which are determined by their respective values of the van der Waals constant C_6^i. For noble-gas perturbers an approximate expression for C_6^i is

$$C_6^i \cong e^2 \langle r^2 \rangle_i \alpha_d, \tag{13}$$

where e is the charge of the electron, $\langle r^2 \rangle_i$ is the average value of the excited electron's orbital radius squared, and α_d is the static dipole polarizability of the perturber. (This equation is discussed further in the Appendix.)

After a collision the atom is assumed to be left in the same superposition state but with a phase shift of its oscillating dipole moment. The phase shift for a particular collision is calculated using

the formula

$$\eta = \frac{1}{\hbar}\int_{-\infty}^{\infty}[V_u(R) - V_l(R)]\,dt. \tag{14}$$

If the trajectories of the particles are not altered by the collision, then the integral in Eq. (14) can be performed analytically for a given impact parameter and average relative velocity. Each phase shift is weighted by the probability for a collision at that impact parameter, and then this result is averaged. The averaged results gives a rate of exponential damping of the dipole moment

$$\Gamma = 4.06(C_6/\hbar)^{2/5}\overline{V}^{3/5}N \propto (\langle r^2\rangle_u - \langle r^2\rangle_l)^{2/5}, \tag{15}$$

where $C_6 = C_6^u - C_6^l$, $\overline{V}$ is the average relative velocity, and N is the number density of perturber atoms.[29] The second line in Eq. (15) indicates explicitly the dependence of Γ on the atomic states involved in the transition.

The results of the calculation are presented in the fifth column of Table II. In general, the theory predicts the observed decay times within a factor of two. The theory overestimates T_2 but shows the general trend of the experimental data. According to this model the shorter wavelength transitions damp more quickly due to the larger difference between the van der Waals constants for the upper and lower states. Also, according to this model, argon is a very effective perturber because of its high dipole polarizability despite its low average thermal velocity.

As a further test of this theoretical model the lifetimes of the dipole moments were calculated for various transitions in sodium perturbed by argon. Flusberg *et al.*[9] have recently observed photon echoes in Na-argon mixtures and have measured T_2 for a number of transitions. The results of theory and experiment are listed in Table III. The calculation appears to describe accurately the dependence of T_2 on principal quantum number and orbital angular momentum of the atomic states, though it is consistently large by a factor of 1.5. Previous line-broadening measurements also have indicated that the sodium-argon interaction is well described by a van der Waals potential.[32]

The accuracy of this theory is limited by a number of assumptions which are employed to simplify the calculations. Two approximations are the linear-path approximation and not including the effect of repulsive forces at small impact parameter. Both of these approximations will be worse for the lighter noble gases, helium and neon.[29] This theory also ignores the anisotropy of the true van der Waals potential and neglects treating spatial degeneracy in the levels of the radiating atom. Schuller and Behmenburg[30] state, however, that explicitly treating these properties of the potential and radiating atom does not alter the theoretical results significantly in most cases. Collision induced transitions are also ignored, but since these take place at impact parameters where the van der Waals interaction has already totally dephased the dipole moment,[9] this approximation is most likely not the cause of the discrepancy with experiment.

The simple theory predicts the general trend of the experimental data; the results are surprisingly accurate for such a simple model. Such a theory is useful for understanding the qualitative behavior of the photon-echo decay times as a function of atomic transition and perturber species and, in certain cases, may supply useful quantitative predictions of the observed decay times.

C. Limitations of the single-exponential decay approximation

If one treats in detail the spatial degeneracy of the levels involved in the photon-echo emission then the final expression for the echo signal is composed of a sum of terms each relaxing at a different rate.[22,33] Each term represents contributions to the echo amplitude from different multipole moments excited by the laser pulses. If the probability of a collision is independent of direction, then each multipole moment decays independently and in general at a different rate.[34] Thus in some cases the decay rate of the photon echo should not necessarily equal the dipole-moment decay rate measured in line-broadening experiments.

The presence of a magnetic field in these experiments complicates a rigorous theoretical treatment of spatial degeneracy. Since the g factors of the ground and excited states are usually different, even small magnetic fields mix the multipole moments created by the incident pulses, thus complicating a theoretical treatment of the relaxation process.[35] The author is not aware of any theoretical treatments of photon-echo relaxation under these conditions.

Since multiexponential decay was not noticed in these experiments, the next step should be a theoretical calculation of the expected differences between the various multipole-moment decay rates. Such a calculation could probably use as its basis the treatment of multipole relaxation and transfer rates developed by Carrington *et al.*[36]

ACKNOWLEDGMENTS

I wish to thank Professor Isaac Abella for his constant support and encouragement throughout the course of this work and Dr. Steve Aoki, Dr. Charles Clark, and Professor Gordon Berry for many helpful discussions. This work was supported in part by the NSF, Division of Materials Research under DMR-17546 and by the Louis Block Fund at the University of Chicago. This work was submitted to the Department of Physics, University of Chicago, in partial fulfillment of the requirements for the Ph.D. degree.

APPENDIX

In order to calculate the damping times listed in Tables II and III the van der Waals constant in Eq. (12) must be evaluated for both levels in the radiating atom. If the spacing of energy levels in the perturber is larger than the energy-level difference in the radiating atom, then C_6^i can be approximated as

$$C_6^i \cong e^2\langle r^2\rangle_i \alpha_d \,, \tag{A1}$$

where e is the charge of the electron, $\langle r^2\rangle_i$ is the average value of the electron orbital radius squared, and α_d is the static dipole polarizability of the perturber atom ground state.[29]

The quantity $\langle r^2\rangle_i$ can be approximated using the expression

$$\langle r^2\rangle_i = \tfrac{1}{2} a_0^2 (n^*)^2 [5(n^*)^2 + 1 - 3l(l+1)] \,, \tag{A2}$$

where n^* is the effective quantum number, l is the orbital quantum number, and a_0 the Bohr radius.[29]

The static dipole polarizabilities of the noble-gas ground states were taken from Table III in the paper by Dehmer *et al.*[37]

The value of C_6^i calculated using the formulas listed above agree well with estimates of the value of C_6^i obtained from low-energy atom-atom scattering data.[38]

[1] I. D. Abella, N. A. Kurnit, and S. R. Hartmann, Phys. Rev. 141, 391 (1966).
[2] In solids, for example, N. Takeuchi and A. Szabo, Phys. Lett. A 50, 361 (1974); Joseph B. W. Morsink, Thijs J. Aartsma, and Douwe A. Wiersma, Chem. Phys. Lett. 49, 34 (1977).
[3] C. K. N. Patel and R. E. Slusher, Phys. Rev. Lett. 20, 1087 (1968).
[4] R. G. Brewer and R. L. Shoemaker, Phys. Rev. Lett. 27, 631 (1971).
[5] S. S. Alimpiev and N. V. Karlov, Sov. Phys.-JETP 36, 255 (1973).
[6] C. V. Heer and R. J. Nordstrom, Phys. Rev. A 11, 536 (1975).
[7] P. R. Berman, J. M. Levy, and R. G. Brewer, Phys. Rev. A 11, 1688 (1975).
[8] R. G. Brewer and A. Z. Genack, Phys. Rev. Lett. 16, 659 (1977).
[9] A. Flusberg, T. Mossberg, and S. R. Hartmann, Opt. Commun. 24, 207 (1978).
[10] R. L. Shoemaker and F. A. Hopf, Phys. Rev. Lett. 33, 1527 (1974).
[11] L. Q. Lambert, Phys. Rev. B 7, 1834 (1973).
[12] T. Baer and I. D. Abella, Phys. Rev. 16, 2093 (1977).
[13] S. Aoki, Phys. Rev. A 20, 2013 (1979).
[14] T. Baer and I. D. Abella, Opt. Lett. 3, 170 (1978).
[15] H. G. Kuhn, *Proceedings of the International Conference on Optical Pumping and Atomic Line Shape* (Pantswowe Wydawnictwo Naukowe, Warsaw, 1968).
[16] W. R. Hindmarsh and K. A. Thomas, Proc. Phys. Soc. London A 77, 1193 (1961); D. N. Stacey and J. M. Vaughan, Phys. Lett. 11, 105 (1967).
[17] J. R. Dixon and F. A. Grant, Phys. Rev. 107, 118 (1957).
[18] A. V. Phelps, Phys. Rev. 99, 1307 (1955).
[19] J. L. Delcroix, C. M. Ferreira, and A. Ricard, in *Principles of Laser Plasmas*, edited by G. Bekefi (Wiley, New York, 1976), p. 159.
[20] L. Allen and J. H. Eberly, *Optical Resonance and Two Level Atoms* (Wiley, New York, 1975).
[21] M. O. Scully, M. Stephen, and D. C. Burnham, Phys. Rev. 171, 213 (1968).
[22] T. Baer, Phys. Rev. A 18, 2570 (1978).
[23] M. Littman and H. Metcalf, Appl. Opt. 17, 2224 (1978).
[24] T. W. Hänsch, Appl. Opt. 11, 895 (1972).
[25] C. E. Moore, *Atomic Energy Levels*, Natl. Bur. Stand. (U.S.) Circ. No. 467, 1958, Vol. I.
[26] W. L. Wiese, M. W. Smith, and B. M. Glennon, *Atomic Transition Probabilities*, National Standard Reference Data Series, NBS-4 (U.S. GPO, Washington, D. C., 1966).
[27] M. W. Zemansky, Phys. Rev. 34, 213 (1929).
[28] P. R. Berman, Appl. Phys. 6, 283 (1975).
[29] W. Hindmarsh and J. M. Farr, Prog. Quantum Electron. 2, 139 (1972).
[30] F. Schuller and W. Behmenburg, Phys. Rep. 12, 273 (1974).
[31] K. Lang, Acta Phys. Austriaca 5, 376 (1951).
[32] A. C. G. Mitchell and M. W. Zemansky, *Resonance Radiation and Excited Atoms* (Cambridge University, Cambridge, England, 1971), Chap. IV.
[33] I. V. Yevseyev and V. M. Yermachenko, Phys. Lett. A 60, 187 (1977); C. H. Wang, Phys. Rev. B 1, 156 (1970).
[34] A. Ben-Reuven, Phys. Rev. 141, 34 (1966).
[35] U. Fano and J. H. Macek, Rev. Mod. Phys. 45, 553 (1973).
[36] C. G. Carrington, D. N. Stacey, and J. Cooper, J. Phys. B 6, 417 (1973).
[37] J. L. Dehmer, M. Inokuti, and R. P. Saxon, Phys. Rev. A 12, 102 (1975).
[38] R. B. Bernstein and J. T. Muckerman, Adv. Chem. Phys. 12, 389 (1967).